

# CoINR: COMPRESSED IMPLICIT NEURAL REPRESENTATIONS

**Anonymous authors**

Paper under double-blind review

## ABSTRACT

Implicit Neural Representations (INRs) are increasingly recognized as a versatile data modality for representing discretized signals, offering benefits such as infinite query resolution and reduced storage requirements. Existing signal compression approaches for INRs typically employ one of two strategies: 1. direct quantization with entropy coding of the trained INR; 2. deriving a latent code on top of the INR through a learnable transformation. Thus, their performance is heavily dependent on the quantization and entropy coding schemes employed. In this paper, we introduce **CoINR**, an innovative compression algorithm that leverages the patterns in the vector spaces formed by weights of INRs. We compress these vector spaces using a high-dimensional sparse code within a dictionary. Further analysis reveals that the atoms of the dictionary used to generate the sparse code do not need to be learned or transmitted to successfully recover the INR weights. We demonstrate that the proposed approach can be integrated with any existing INR-based signal compression technique. Our results indicate that **CoINR** achieves substantial reductions in storage requirements for INRs across various configurations, outperforming conventional INR-based compression baselines. Furthermore, **CoINR** maintains high-quality decoding across diverse data modalities, including images, occupancy fields, and Neural Radiance Fields.

## 1 INTRODUCTION

Despite the fact that all naturally occurring signals observed by humans are continuous, capturing these signals through digital devices requires their discretization. For example, an image of a mountain is processed and stored in a discretized format. A primary reason for this approach is to conserve storage space; storing signals with high precision in an almost continuous manner would necessitate a substantial amount of storage. Consequently, the digital representation of signals in a discretized form is both practical and essential. For instance, it is estimated that over 400TB of data is created every day (Duarte, 2024). Moreover, humans share their captured signals through various mediums on a daily basis. Therefore, data compression becomes essential for efficient and reliable transmission.

Traditional signal compression techniques often rely on classic signal processing methods and are typically unimodal. For example, JPEG (Wallace, 1992), designed for photographic images, and is unsuitable for audio files. Similarly, audio compression standards like MP3 or AAC (Brandenburg, 1999) are optimized for sound and are not applicable to images. With the advancements of neural networks, researchers have explored compressing signals using neural methods, predominantly through mechanisms based on autoencoders (Alexandre et al., 2018; Cheng et al., 2019; Theis et al., 2022). In these systems, the encoder transforms the signal into a latent vector, which the decoder then uses to reconstruct the original signal. While autoencoder-based methods effectively encode signals into latent vectors, they are generally designed for images or another single modality. Adapting these methods to different data modalities not only requires training on a large corpus of data specific to those modalities but also a specialized autoencoder architecture tailored to handle the data effectively.

In recent years, there has been a significant surge in interest in representing signals through Implicit Neural Representations (INRs). Unlike large models based on autoencoders, INRs typically consist of multi-layer perceptrons (MLPs) equipped with specialized nonlinearities that differ from the con-

054 ventional nonlinearities used in deep learning. This simplicity and versatility allow INRs to unify  
055 signal representations across diverse data modalities. When signals are represented by INRs, they  
056 are encoded in the MLP’s weights and biases. For instance, in image transmission, instead of using  
057 conventional JPEG encoding, the weights and biases of the MLP are transmitted by a transmitter  
058 (TX). A receiver (RX) can then feed the coordinates into the MLP and decode the image. The pri-  
059 mary advantage of INRs lies in their ability to represent signals with high fidelity while utilizing  
060 fewer parameters than parameter-heavy autoencoder-based mechanisms.

061 Recent advances in INR-based signal compression include COIN (Dupont et al., 2021), COIN++  
062 (Dupont et al., 2022), and INRIC (Strümpfer et al., 2022). COIN pioneered the application of INRs  
063 for image compression. Building on this, COIN++ and INRIC introduced quantization and entropy  
064 coding to improve compression efficiency. Both approaches also focus on enhancing the general-  
065 ization capabilities of INRs through meta-learning techniques. Additionally, COIN++ incorporates  
066 latent modulations discovered via a learnable transformation applied on top of the INR model. How-  
067 ever, COIN++ requires transmitting the base INR and the learned transformation a priori, in addition  
068 to the latent modulations for signal decoding. None of the existing methods, however, have explored  
069 fundamentally compressing the INR by identifying patterns within its parameter space before ap-  
070 plying standard techniques such as quantization and entropy coding.

071 In our work, named **CoINR**, we build upon the observed behaviors of the vector spaces generated  
072 by the weights in an INR. We integrate compressed sensing algorithms into the INR-based compres-  
073 sion pipeline, proposing a mechanism that obtains a higher-dimensional sparse code for the weight  
074 vectors without requiring any learnable transformations. Furthermore, based on the Central Limit  
075 Theorem (CLT) (Zhang et al., 2022), we show that the transformation matrix need not be transmit-  
076 ted for successful decoding of weight spaces. This further enhances and simplifies the decoding  
077 process. Consequently, **CoINR**, as a fundamental compression technique built on the observations  
078 of weights spaces, achieves superior compression and higher decoding quality for each data modal-  
079 ity compared to the baselines. Moreover, it can be easily embedded into any INR-based signal  
080 compression algorithm.

## 081 2 RELATED WORKS

### 082 2.1 IMPLICIT NEURAL REPRESENTATIONS

083  
084 INRs have recently gained considerable attention in the computer vision community due to their  
085 streamlined network architectures and improved performance in various vision tasks compared to  
086 traditional, parameter-heavy models (Sitzmann et al., 2020; Saragadam et al., 2023; Hao et al.,  
087 2022). This surge in interest followed the advent of Neural Radiance Fields (NeRF) (Mildenhall  
088 et al., 2021), which has inspired a plethora of subsequent studies (Zhu et al., 2023; Rabby & Zhang,  
089 2023). Further research has explored the pivotal role of different activation functions in INRs (Sitz-  
090 mann et al., 2020; Saragadam et al., 2023; Ramasinghe & Lucey, 2022; Tancik et al., 2020). More-  
091 over, INRs have transformed into a unified data modality that integrates various types of visual  
092 information into a consistent format. More recent studies have investigated the use of INRs for im-  
093 age classification by transforming standard image formats into INRs and training classifiers directly  
094 on the INRs’ weights and biases (Shamsian et al., 2024). These innovative approaches have show-  
095 cased the potential of INRs to significantly reduce the dimensionality and computational complexity  
096 typically associated with conventional image processing techniques.

### 097 2.2 SIGNAL COMPRESSION

098  
099 Signal compression is crucial for reducing bandwidth needs and saving storage space. With the  
100 rise of deep learning, signal compression has evolved into two main approaches: rule-based (tradi-  
101 tional) and learning-based methods. Traditional compression methods, such as JPEG for images and  
102 MP3 for audio, rely on algorithmic techniques tailored to specific signal types. JPEG minimizes re-  
103 dundancies using the discrete cosine transform (Raid et al., 2014), while MP3 (Brandenburg, 1999)  
104 employs a psycho-acoustic model that enhances compression by removing inaudible sounds through  
105 auditory masking. On the other hand, deep learning-based techniques use models trained on vast  
106 datasets, adapting to a wide range of signals without predefined algorithms. These methods offer  
107 flexibility but require different architectures for each data modality, presenting unique challenges.

In this landscape, INRs stand out as a potential universal signal representer. INRs can handle various data types through a unified framework, promising a versatile solution in the realm of signal compression.

### 2.3 COMPRESSED SENSING

Compressed sensing is a field that capitalizes on the inherent sparsity of data to capture information efficiently. In digital imaging, not every pixel is crucial for accurate image reconstruction. Although images appear dense in pixel space, they exhibit considerable redundancy when transformed into different basis functions. This sparsity is exploited by compressed sensing algorithms to reconstruct the original image from fewer sampled data points. These algorithms employ optimization techniques and linear algebra to solve underdetermined systems, revolutionizing data acquisition in areas such as medical imaging and signal processing. Dictionary learning, integral to compressed sensing, seeks sparse representations of data using dictionary elements or atoms that capture the data’s intrinsic structure. These atoms are either predefined or adaptively learned. Compressed sensing’s versatility is evident in its applications across various domains, such as image and video compression (Zhou & Yang, 2024), medical image encryption (Jiang et al., 2024), and classification tasks (Liu & Fieguth, 2010; Kapoor et al., 2012; Hsu et al., 2009; Hu & Tan, 2018). It also addresses inverse vision problems like image inpainting (Seemakurthy et al., 2020), deblurring (Ma et al., 2013; Hu et al., 2010), and super-resolution (Ayas & Ekinci, 2020). Recent efforts have merged dictionary learning with deep learning to tackle more complex computer vision challenges, including image recognition (Tang et al., 2020), denoising (Zheng et al., 2021), and scene recognition (Liu et al., 2018). These developments underscore compressed sensing’s transformative impact on computer vision.

Our work, **CoINR**, is pioneering the application of compressed sensing principles to INRs. By leveraging these principles alongside the structural distributions of INR weights, **CoINR** identifies redundancies in these spaces, resulting in substantial compression improvements.

## 3 METHOD

### 3.1 SIGNAL REPRESENTATION THROUGH INRS

Mathematically, an INR can be defined by a function  $G_\theta$ , where  $\theta$  are the optimizable parameters of the neural network. The input and output dimensions of  $G_\theta$  vary for different data modalities. In general,  $G_\theta$  acts as a mapping from an  $a$ -dimensional input coordinate space to a  $b$ -dimensional output signal space, described mathematically as:

$$G_\theta : \mathbb{R}^a \rightarrow \mathbb{R}^b.$$

For instance, for RGB images,  $a = 2$  and  $b = 3$ , while for audio signals,  $a = 1$  and  $b = 1$ . In this architecture, the output of the  $i^{\text{th}}$  layer, which feeds into the  $(i + 1)^{\text{th}}$  layer, can be expressed as  $\sigma(W^{(i)}y^{(i)} + b^{(i)})$ . Here,  $\sigma$  denotes the activation function, and  $y^{(i)}$  represents the output from the preceding layer. Furthermore, the choice of activation function ( $\sigma$ ) plays a critical role in shaping the neural network’s ability to model complex functions, as explored in various studies (Sitzmann et al., 2020; Ramasinghe & Lucey, 2022; Saragadam et al., 2023; Tancik et al., 2020).

### 3.2 EXPLORING THE COMPRESSIBILITY

According to compressed sensing theory, most real-world signals display sparsity when transformed into an appropriate domain, meaning they can be accurately represented with fewer measurements than traditionally required. Furthermore, real-world signals can be compressed through a set of basis functions, and the coefficients of these functions are derived by minimizing the reconstruction loss. The core concept of INRs involves encoding signals into the weights and biases of an MLP. This process can be viewed as a classical domain transformation technique where pixel values are reconstructed by feeding the corresponding coordinates through the MLP. Unlike predefined signal transformers like Fourier (Chandrasekharan, 2012) and DCT (Khayam, 2003), the MLP attempts to minimize the reconstruction loss through backpropagation to find the transformation. The learned representation of the signal resides in another domain. Given that real-world signals inherently

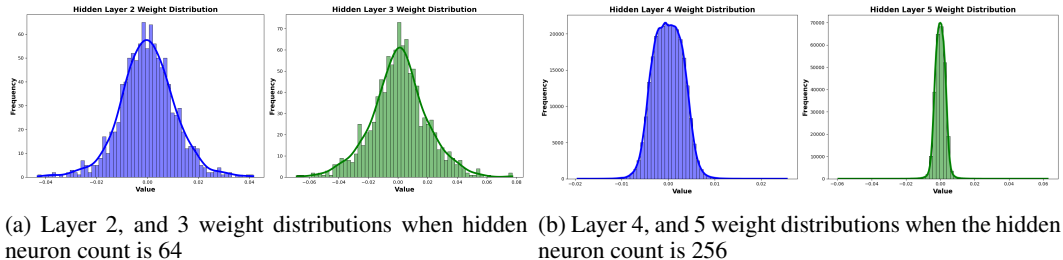


Figure 1: **Weight distribution of INRs follows a Gaussian distribution:** A randomly chosen image from Kodak dataset was fitted through an INR.

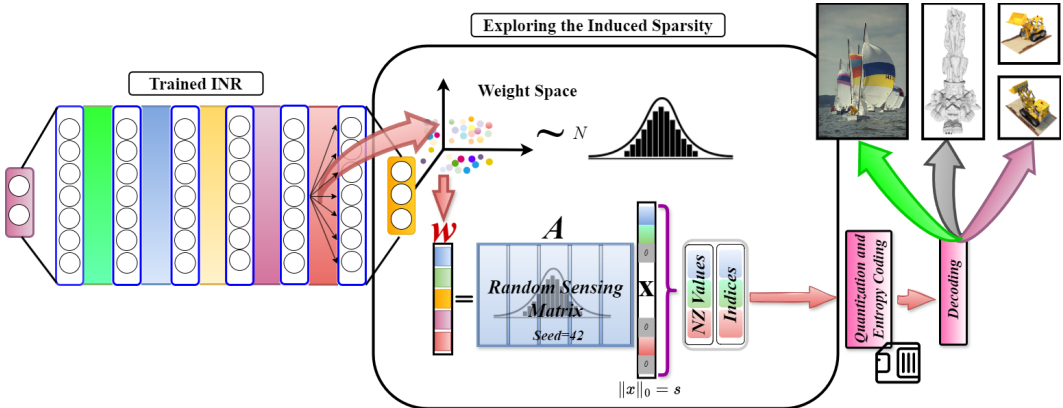


Figure 2: **The proposed CoINR compression algorithm** Standard compression techniques for INRs typically involve direct quantization and entropy coding of their weights. However, since natural signals exhibit inherent compressibility in a dictionary, the characteristics that aid in the compressibility of the weight space of an INR are discovered through the Gaussian nature of the weight space. Therefore, **CoINR** employs  $L_1$  minimization to identify a higher-dimensional sparse code. Furthermore, based on the weight space observations and the Central Limit Theorem (CLT), we simplify the encoding and decoding process using a random sensing matrix controlled by a seed. Subsequently, only the non-zero (NZ) values and their corresponding indices are quantized and entropy coded.

exhibit sparsity in transformed domains, we hypothesize that this sparsity can be explored within the MLP’s weights. If we can identify where this sparse nature is hidden within the weight space, we could achieve further compression on INRs compared to the baselines. However, identifying this sparse representation within the weights is not straightforward. We believe there are two main approaches to achieving a sparser representation, each with its own challenges and considerations.

The first approach involves either promoting or enforcing a specified level of sparsity in the weights during the training of an INR. Promoting sparsity can generally be achieved by incorporating  $L_1$  regularization on the model parameters, which encourages the model to set as many weights as possible to zero, thereby creating a sparse representation. Enforcing a specified level of sparsity can be achieved through model pruning, where weights deemed insignificant are pruned or eliminated during the training process. Despite our efforts using these techniques, we observed that  $L_1$  regularization results in a higher level of sparsity within the weights but fails to showcase a clear pattern of sparsity levels for natural images. When it comes to model pruning, we employed both structured and unstructured pruning of weights. We noted that both methods led to significant performance degradation for certain data modalities, particularly for occupancy fields. Moreover, only a small pruning percentages resulted in satisfactory performance for signal representation. For applications that require a high level of generalization, such as NeRFs, the pruning approach did not generalize well, indicating its limitations in achieving a balance between sparsity and performance.

216 The second approach seeks to uncover the inherent structures within the weights that aid in INR  
 217 compression. This involves identifying patterns or regularities that can be exploited to reduce the  
 218 dimensionality of the representation without sacrificing performance. We examined this from a  
 219 dimensionality reduction perspective; however, the weight space in reduced dimensions did not  
 220 reveal clear patterns, even across different natural images. However, we observed that the weight  
 221 space of an INR follows a normal distribution for every instance of every data modality. Figure 1  
 222 shows the weight distribution of hidden layers of an INR when an image is encoded into it. Our  
 223 observations are further confirmed by analysis done in [Sitzmann et al. \(2020\)](#). This suggests that  
 224 INRs share a common pattern across different data modalities, showcasing a potential pathway for  
 225 a fundamental compression.

226 Given that each weight vector of an INR exhibits Gaussian behavior, we seek a higher-dimensional  
 227 but sparse equivalent through a dictionary learning-based approach. Let us denote  $\mathbf{w} \in \mathbb{R}^{k_1}$  as  
 228 a hidden weight vector,  $\mathbf{A} \in \mathbb{R}^{k_1 \times k_2}$  as a dictionary, and  $\mathbf{x} \in \mathbb{R}^{k_2}$  as the corresponding sparse  
 229 vector. In search of a sparse representation, according to standard compressed sensing, we can write  
 230  $\mathbf{w} = \mathbf{Ax}$ , where  $\|\mathbf{x}\|_0 < k_1$ . To discover the sparse code  $\mathbf{x}$ , the best and most efficient choice  
 231 is  $L_1$  minimization, as  $L_0$  minimization iterates through all possible combinations and is therefore  
 232 not efficient. However, the problem arises with the sensing matrix, commonly referred to as the  
 233 dictionary  $\mathbf{A}$ . Although we could use either a dictionary learning-based approach for learning basis  
 234 functions for the dictionary or a deep learning-based learnable transformation, these approaches  
 235 would be time-consuming. Furthermore, a TX needs to transmit the learned dictionary alongside  
 236 the obtained sparse codes. Further exploration of the weight space revealed that the dictionary does  
 237 not need to be learned or even transmitted.

238 As we have confirmed, the weights are normally distributed. According to the Central Limit Theo-  
 239 rem (CLT), a normally distributed random variable can be produced through a finite linear combi-  
 240 nation of any random variables. In summation form, this can be expressed as:  $w_i = \sum_{j=1}^{k_2} A_{ij}x_j$ ,  
 241 where  $w_i$  is the  $i$ -th element of the weight vector  $\mathbf{w}$ ,  $A_{ij}$  is the element in the  $i$ -th row and  $j$ -th  
 242 column of the sensing matrix  $\mathbf{A}$ , and  $x_j$  is the  $j$ -th element of the vector  $\mathbf{x}$ . To satisfy the CLT, the  
 243 number of terms in the summation, which is  $k_2$ , should be sufficiently large. Therefore, considering  
 244 all elements of the weight vector  $\mathbf{w}$ , this can be compactly written as  $\mathbf{w} = \mathbf{Ax}$ . As we now under-  
 245 stand the structure of the sensing matrix, which is a random matrix, the appropriate coefficients of  
 246 those random vectors can be learned through the  $L_1$  minimization discussed earlier by leveraging  
 247 dictionary learning algorithms such as matching pursuit or its variants. Therefore, the optimization  
 248 problem can be written as,  $\min \|\mathbf{x}\|_1$  subject to  $\mathbf{w} = \mathbf{Ax}$ . For convenience, let us denote  $\|\mathbf{x}\|_0$  as  
 249  $s$ . A further constraint to the above optimization procedure is that when the sparse code  $\mathbf{x}$  is found,  
 250 we need to store not only its non-zero elements but also the corresponding indices. Therefore, the  
 251 above  $L_1$  minimization is solved with  $2s < k_1$ . We do not apply our compression algorithm to the  
 252 biases on the INR as the size of bias vectors is very small compared to those of the weight matrices.

253 Instead of saving  $k_1$  floating-point numbers for  $\mathbf{w}$ , we now only need to save  $2s$  elements:  $s$  elements  
 254 are floating-point numbers representing the non-zero values in the sparse code, and the remaining  
 255  $s$  elements are integers that give the indices of those non-zero values. The indices can often be  
 256 represented with 16-bit precision, unlike the non-zero values in the sparse code, which require 32-  
 257 bit floating-point precision. At the RX end,  $\mathbf{x}$  must be converted back to  $\mathbf{w}$ . This requires the  
 258 sensing matrix  $\mathbf{A}$ , which is random and must be controlled by a seed to reproduce the exact  $\mathbf{w}$  using  
 259  $\mathbf{w} = \mathbf{Ax}$ . Thus, the receiver only needs  $\mathbf{x}$  to obtain  $\mathbf{w}$ .

260 This process can be viewed as a method of uncovering the inherent sparsity within natural signals, as  
 261 represented through the weight space of INRs. As we hypothesized, the ability to condense natural  
 262 signals into a dictionary hinges on identifying specific patterns encoded within the weights of INRs.  
 263 Once the non-zero elements of the sparse vector are pinpointed, the resulting procedure is virtually  
 264 the same across different INR-based baselines. Our method fundamentally achieves compression by  
 265 delving into the weight spaces to uncover patterns, a step not typically taken by existing baselines.  
 266 A summarization of **CoINR** is illustrated in figure 2. As can be seen from figure 2, **CoINR** is only  
 267 dependent on the weights of the INR and is applied prior to any quantization or entropy coding  
 268 schemes. Therefore, **CoINR** can be applied to any existing INR compression baselines to improve  
 269 their compressibility.



### 270 3.3 HOW MUCH FUNDAMENTAL COMPRESSION DOES **CoINR** ACHIEVE COMPARED TO THE 271 BASELINES? 272

#### 273 3.3.1 STANDARD INRS

274 Consider an INR with  $l$  hidden layers, yielding  $l + 2$  total layers. For simplicity, assume  $k$  neurons  
275 per hidden layer. If the input dimension is  $a$  and the output dimension is  $b$ , the total number of  
276 weight parameters is given by  $\mathcal{T}_s = a \times k + l \times k^2 + b \times k$ . However, **CoINR** modifies this structure  
277 by reducing the parameters from  $\mathcal{T}_s$  in the original network to  $\mathcal{T}_{s\text{CoINR}} = a \times 2s + k \times l \times 2s + b \times 2s$ ,  
278 where  $s \ll k$ . Additionally, unlike COIN++, **CoINR** does not require transmitting any additional  
279 data to recover the original INR weights.  
280

#### 281 3.3.2 TINY INRS

282 Let us define an INR as “tiny” if the number of neurons in a hidden layer, denoted by  $k$ , is less  
283 than 50. In such cases, we aim to achieve a sparse representation where  $2s < k$  and  $\|x\|_0 = s$ .  
284 However, achieving a sparse representation that satisfies  $2s < k$  is often extremely challenging and  
285 typically does not result in effective compression. To overcome this, we exploit the fact that the  
286 weight matrix connecting the  $i^{\text{th}}$  layer to the  $(i + 1)^{\text{th}}$  layer is of dimensions  $k \times k$ . By vectorizing  
287 this weight matrix, we obtain a vector of dimension  $k^2 \times 1$ . Given that  $k^2$  is significantly larger than  
288  $k$ , we can apply our **CoINR** procedure directly to the flattened weight matrix. This strategy leads to  
289 a sparser representation, thereby enhancing compression efficiency for tiny INRs.  
290

#### 291 3.3.3 COIN++

292 In the COIN++ framework, modulation parameters are stored instead of traditional weights and bi-  
293 ases, under the assumption that the base network parameters can be transmitted beforehand. For  
294  $n$  test images, each segmented into  $m$  patches with a latent dimension of size  $d$ , COIN++ necessi-  
295 tates the transmission of  $m \times d$  parameters for reconstructing each image. As the base network in  
296 COIN++ conforms to a standard INR structure, it is amenable to further compression via the **CoINR**  
297 technique. By implementing **CoINR** principles on the modulations in COIN++, the parameter trans-  
298 mission requirement per image can be reduced from  $m \times d$  to just  $2s \times d$ , where  $s \ll m$ . As the  
299 size of each test image and the number of images in the test dataset grow, COIN++ would typically  
300 require the transmission of numerous parameters. However, by leveraging **CoINR**, both the modu-  
301 lations and the base network can be significantly compressed, achieving enhanced compression.  
302

### 303 3.4 QUANTIZATION AND ENTROPY CODING

304 After an INR is trained, its parameters are not immediately saved but are first subject to quantization  
305 (Gray & Neuhoff, 1998). This involves reducing the bitwidths below typical floating-point precision.  
306 Following quantization, the parameters are processed through entropy coding, in our experiments we  
307 utilize Brotli coding (Jones & Jones, 2012; Alakuijala et al., 2018), which allows the compressed  
308 data to be stored or transmitted efficiently. To retrieve the original parameters, the decoder must  
309 reverse the entropy coding and then perform dequantization. In the case of **CoINR**, the compression  
310 process is intensified by utilizing the sparsity induced in the model parameters by natural signals.  
311 Once the sparse code is established, the parameters are quantized and subjected to entropy coding.  
312 The decoder then reverses the entropy coding and dequantizes the data. Finally, the model param-  
313 eters are reconstructed by multiplying them with a random Gaussian matrix, which is determined by  
314 a specific seed.  
315

## 316 4 EXPERIMENTS

### 317 4.1 EXPERIMENTAL SETUP

318 **CoINR**, a novel INR compression algorithm, is predicated on the idea that if natural signals are com-  
319 pressible through a dictionary, then INRs should be similarly compressible. This concept underpins  
320 **CoINR**’s goal to efficiently reduce INR storage requirements while maintaining high fidelity. Our  
321 experiments, conducted using the PyTorch framework following WIRE (Saragadam et al., 2023)  
322 codebase on an NVIDIA RTX A5000 GPU with 24 GB of memory, spanned various data types  
323

including images, occupancy fields, audio, and neural radiance fields. Image encoding metrics involved file size, bits per pixel (bpp) and Peak Signal-to-Noise Ratio (PSNR). Occupancy fields were evaluated using file size and Intersection over Union (IoU), and neural radiance fields were assessed using file size and PSNR. Other than the network configurations mentioned in the paper, for occupancy field evaluation, we utilized an MLP with 128 hidden neurons, and 3 hidden layers. For INRIC, we applied the network hyperparameters specified in its paper. In COIN++, we followed the guidelines in its paper but modified the hidden neuron size to 300. All experiments used Brotli entropy coding with a 16-bitwidth (65536 levels) uniform quantizer.

## 4.2 HOW DO WE FIND $s$ ?

We implemented  $L_1$  minimization using the Orthogonal Matching Pursuit (OMP) algorithm (Tropp & Gilbert, 2007). The OMP algorithm requires the pre-determination of  $s$  before obtaining  $\mathbf{x}$ , and it must adhere to the condition  $2s < k_1$ . If  $2s$  is set too low, it results in inaccurate representations of  $\mathbf{w}$  within the weight space. Therefore, we incrementally increased  $s$  from a low value until  $2s = k_1$  for all KODAK images in the  $C_1$  experiment, as outlined in section 4.3. Our findings suggest that the optimal value of  $s$  for successfully reconstructing the weight space does not depend on the specific image but on the number of neurons in a hidden layer. By adjusting the neuron count, we identified an optimal  $s$  that accurately reconstructs the weight space while satisfying the specified constraint. Extending these experiments to natural signals outside the KODAK dataset confirmed the consistency of our results. Consequently, we have included a regression plot in the supplementary material that details how to determine the optimal  $s$  based on the number of neurons.

## 4.3 IMAGE ENCODING

Representing an image through the weights and biases of a neural network serves as a method of encoding. For our image encoding task, we utilized the KODAK dataset, which includes 24 natural RGB images, each measuring  $768 \times 512$  pixels. We conducted five types of experiments, denoted as  $C_i$ , where  $i$  ranges from 1 to 5, to demonstrate the effectiveness of our proposed method.

Experiment  $C_1$  involved encoding each image in the KODAK dataset using an INR without positional embedding, by varying the number of neurons in each hidden layer. Experiment  $C_2$  mirrored  $C_1$ , but with the variation in the number of hidden layers instead. Experiments  $C_3$  and  $C_4$  implemented the meta-learning approach for INRs proposed in INRIC, without and with positional embedding for the input layer, respectively. For these meta-learning-based experiments, we used the first 12 images of the KODAK dataset for meta-learning and the remaining 12 images for fine-tuning.

Experiment  $C_5$  involved the COIN++ framework, testing both with and without patching. When using patching, we adopted  $32 \times 32$  patches as suggested by COIN++. However, we observed that without patching, even as the latent modulation dimension increased, the average Peak Signal-to-Noise Ratio (PSNR) obtained by COIN++ remained nearly constant. For all image encoding experiments, we used the sinusoidal activation function (see supplementary).

Let us define  $h$  and  $m$  as the number of hidden layers and the number of neurons per hidden layer in an INR, respectively. For experiment  $C_1$ , we configured the INR with settings  $(h, m)$  as  $(2, 32)$ ,  $(3, 64)$ ,  $(3, 128)$ . Experiment  $C_1$  aims to assess the effectiveness of **CoINR** by varying the number of hidden neurons. The results, depicted in figure 3, demonstrate how effectively **CoINR** identifies the compressibility of the weight space. This is indicated by the bits-per-pixel (bpp) values, which reflect the size of the model parameters. For example, representing the KODAK dataset with an average PSNR of 30 dB requires about 3.7 bpp for COIN and 2.0 bpp for INRIC. However, **CoINR** significantly reduces the bpp to approximately 1.7 using the same quantizer and entropy coder. The first configuration in  $C_1$  falls under the category of tiny INRs, underscoring the proposed method’s effectiveness even for compact INRs. As illustrated in figure 3, **CoINR** achieves the same level of PSNR as baselines with a lower bpp for any network configuration. This substantial reduction of bpp across the  $C_1$  experiment showcases the efficiency and compactness achieved by **CoINR**. From  $C_1$ , it can be established that greater compressibility of an INR into a dictionary is possible with an increased number of hidden neurons. Following the conclusions drawn from experiment  $C_1$ , experiment  $C_2$  was designed to explore the impact of increasing the number of hidden layers on the

effectiveness of **CoINR**. The configurations tested in  $C_2$  were  $(h, m) = \{(3, 64), (5, 64), (7, 64)\}$ . As illustrated in figure 3, **CoINR** consistently achieved PSNR levels comparable to baseline methods, but with a reduced bpp. Given that  $C_2$  maintained a constant neuron count at 64, the observed deviations in compression between **CoINR** and INRIC were less significant than those observed in  $C_1$ . This discrepancy can be attributed to the following: an INR configuration with a higher number of neurons (e.g.,  $m = 128$ ), even with fewer hidden layers (e.g.,  $h = 2$ ), possesses more trainable parameters. Consequently, such a model is capable of learning a more robust representation of the image compared to configurations with a larger number of layers but fewer neurons per layer. As a result, the compressible characteristics of the images are more effectively transferred into the model parameters during the INR training process. This leads to a more compressible INR. These findings support the premise that if natural images can be efficiently compressed into a dictionary, the weight space of INRs can also be effectively compressed.

As in previous experiments, each image required separate training of an INR. Experiments  $C_3$  and  $C_4$  address this challenge through meta-learning, with and without positional embedding, respectively. The configuration for these INRs is given by  $(h, m) = \{(3, 32), (3, 64), (3, 96), (3, 128)\}$ . For **COIN++**, the number of layers was set to 5 with MLP's hidden dimension at 300. The latent dimension parameter ( $d$ ) varied as follows:  $d = \{16, 32, 64, 96\}$ . Figure 4 presents the experimental results for  $C_3, C_4,$  and  $C_5$ , illustrating significant compression capabilities of the proposed **CoINR** within a meta-learning framework. Notably, models using positional embedding generally have more parameters than those without.

Comparing the performance of INRIC and **CoINR** without positional embedding schemes, the initial INR configuration shows that **CoINR** exhibits a lower bpp for the same average PSNR. Generally, as bpp increases, the representation capacity of the INR enhances, leading to more robust image representation. At higher bpp values, the **CoINR** graphs demonstrate a greater deviation from the INRIC graphs, a phenomenon that can be explained by the aforementioned logic.

In the case of **COIN++**, the approach focuses on fine-tuning only the modulations using their proposed meta-learning method. However, since fine-tuning encodes natural signals within these modulations, they should be compressible via a dictionary. Due to patching, each KODAK test image results in a  $d \times 384$  matrix. Our experiments reveal that these modulations encode hidden redundancies in natural signals. For instance, to achieve an average PSNR of approximately 24.2 dB, **COIN++** requires more than 1.5 bpp; however, the same PSNR can be achieved with **COIN++** using just under 1 bpp by exploiting the hidden sparsity in its modulations through our proposed approach. Therefore, when a high-capacity model effectively represents a signal, it must encapsulate this sparsity within its weight and bias spaces. **CoINR** explores and removes redundancies in these parameters, retaining only essential information. Figure 5 showcases the decoded images by **CoINR** alongside

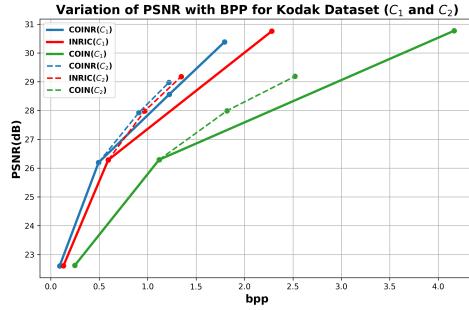


Figure 3: **Experiments  $C_1$  and  $C_2$ : Identifying compressible INR combinations.** The **CoINR** approach demonstrates that configurations in  $C_1$  are more compressible than those in  $C_2$ . Furthermore, in both configurations **CoINR** achieves lower bpp while maintaining the PSNR values.

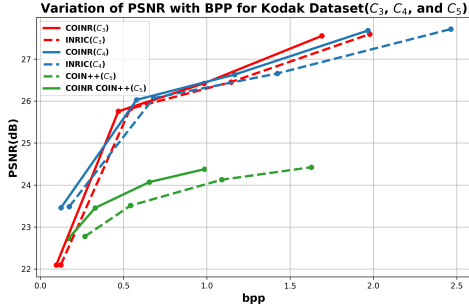


Figure 4: **Experiments  $C_3, C_4,$  and  $C_5$ : Identifying compressible INR combinations under Meta-Learning.** Meta-learning approaches have been introduced for INRs to enhance their generalization abilities and achieve faster convergence. When assessing induced sparsity in the weight space, **CoINR** demonstrates a significant reduction in bpp values while maintaining nearly the same PSNR performance as the baselines.



with the INR based image compressors. Decoded PSNR, BPP, and file size are displayed in the first, second, and third rows of the text boxes

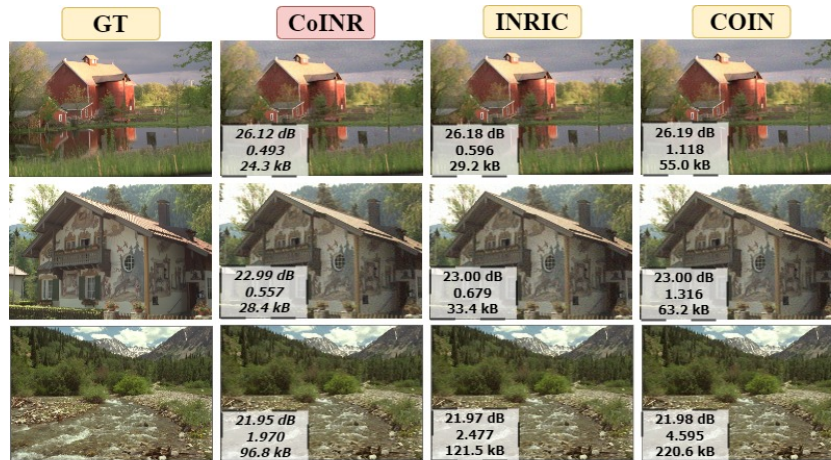


Figure 5: **Results for image encoding experiment.** CoINR compresses the INR into a dictionary, significantly reducing the storage required compared to baseline INR image compressors. The results demonstrate that the decoded representations undergo a very negligible loss in PSNR, which is minimal considering the substantial storage space saved.

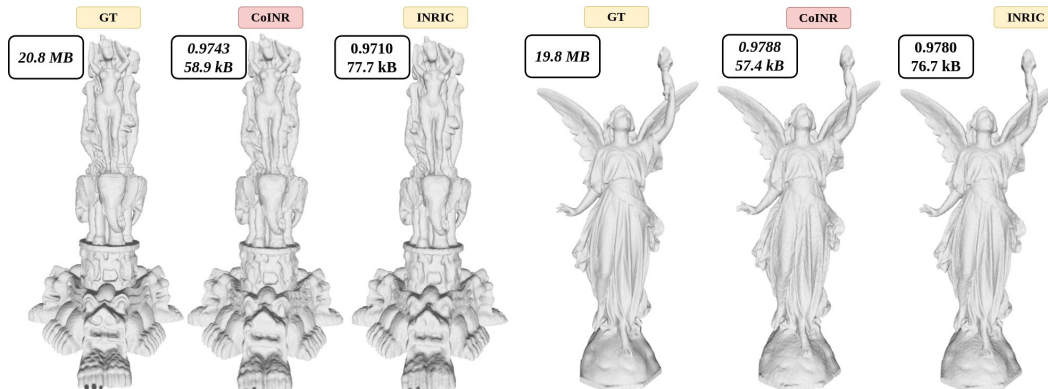


Figure 6: **Results for occupancy fields encoding experiment.** The results clearly demonstrate that CoINR achieves the smallest file size and the highest accuracy metric for every shape in the tested dataset. The significant compression obtained by our algorithm suggests that occupancy fields, when represented using an INR, can be more efficiently compressed into a dictionary compared to images. This may be attributed due to the inherent redundancies present in the occupancy fields.

#### 4.4 OCCUPANCY FIELDS ENCODING

Occupancy fields are represented by binary values, either 1 or 0, where 1 denotes that the signal lies within a specified region and 0 indicates its absence. Another variant of occupancy volumes stores not only the presence or absence of a signal but also the color at that location. Typically, occupancy fields consume more space than other data modalities. However, they can be represented with higher accuracy and lower storage requirements using INRs. In this experiment, we followed the sampling procedure described in Saragadam et al. (2023). Occupancy fields can be thought of as representations of three-dimensional objects, capturing natural signals. Despite following the sampling procedure, redundancies may exist that are not essential for representing the occupancy volume. Identifying these redundancies can reduce storage requirements. However, identifying them in the spatial domain (xyz) requires domain-specific algorithms, as described in section 1.

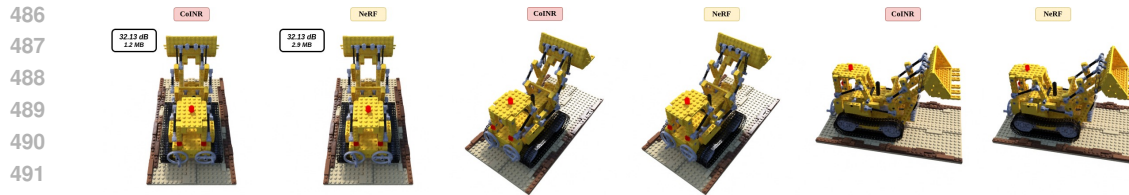


Figure 7: **Results for NeRF compression:** **CoINR** compresses the radiance field without any loss in PSNR while significantly reducing storage requirements.

As INRs serve as unified data modality representors, these redundancies must be encapsulated within its weights space. **CoINR** fundamentally compresses the INRs into a dictionary regardless of the data modality; therefore, indeed it is equally applicable to occupancy fields. To validate this hypothesis for occupancy fields, two experiments were conducted using shapes from the Stanford shape dataset ([Stanford University Computer Graphics Laboratory](#)). Figure 6 showcases the decoded **CoINR**'s representations for 'Thai Statue' (first volume) and 'Lucy' (fourth volume) datasets alongside the existing INR-based occupancy compressor. We use the Gaussian activation function for this task (see supplementary). The first value and second value in each text box represent the IoU metric and storage requirement, respectively, except for GT.

#### 4.5 NEURAL RADIANCE FIELDS ENCODING

NeRF can be considered a novel view generator when it is trained with a sufficient number of training views, along with their corresponding positions and directions. Fundamentally, once trained, a NeRF is an INR. Therefore, the information encoded in its weights for generating novel views can be compressed into a dictionary. Figure 7 presents the results obtained with the proposed **CoINR**. As shown, **CoINR** achieves more than 50% compression while maintaining the same PSNR. These results further confirm the applicability of **CoINR** for compressing INRs across different data modalities. We used the ReLU-PE activation for encoding NeRFs.

#### 4.6 ADDITIONAL MATERIALS

The pseudocode for **CoINR**, additional results, and ablation studies on finding  $s$  are available in the supplementary material.

## 5 CONCLUSION

Implicit Neural Representations (INRs) have emerged as a promising framework for unified data modality representation. Several studies have explored the potential for compressing images, occupancy fields, and audio using INRs. However, none of these methods have investigated whether the INR itself can be compressed prior to quantization and entropy coding. As natural signals can be efficiently compressed in bases of transformed domains due to their sparsity—allowing for higher accuracy and lower storage requirements—we hypothesize that a similar compressible nature must also exist in the INR once it is trained. With the discovery that weight vectors in the weight space tend to adhere to a Gaussian distribution, we propose **CoINR**, which compresses any INR in a dictionary. Furthermore, we demonstrate that this dictionary does not need to be learned but can instead be generated using a seed. We compare our findings with standard INR compressors for images, occupancy fields, and neural radiance fields. **CoINR** achieves fundamental compression for any INR, independent of other post-processing methods such as quantization and entropy coding, and it showcases significantly lower storage requirements and higher fidelity across various data modalities. Through our experiments, we observed that the INR can be more compressed when a more robust representation of the signal is learned. Additionally, some data modalities exhibit greater compressibility than others. We firmly believe this research will aid other researchers in exploring more patterns in the weight spaces of INRs and in developing operators and transforms for INR.

## REFERENCES

- 540  
541  
542 Jyrki Alakuijala, Andrea Farruggia, Paolo Ferragina, Eugene Kliuchnikov, Robert Obryk, Zoltan  
543 Szabadka, and Lode Vandevenne. Brotli: A general-purpose data compressor. *ACM Transactions*  
544 *on Information Systems (TOIS)*, 37(1):1–30, 2018.
- 545 David Alexandre, Chih-Peng Chang, Wen-Hsiao Peng, and Hsueh-Ming Hang. An autoencoder-  
546 based learned image compressor: Description of challenge proposal by nctu. In *Proceedings of*  
547 *the IEEE Conference on Computer Vision and Pattern Recognition Workshops*, pp. 2539–2542,  
548 2018.
- 549 Selen Ayas and Murat Ekinici. Single image super resolution using dictionary learning and sparse  
550 coding with multi-scale and multi-directional gabor feature representation. *Information Sciences*,  
551 512:1264–1278, 2020.
- 552  
553 Karlheinz Brandenburg. Mp3 and aac explained. In *Audio Engineering Society Conference: 17th*  
554 *International Conference: High-Quality Audio Coding*. Audio Engineering Society, 1999.
- 555 Komaravolu Chandrasekharan. *Classical Fourier Transforms*. Springer Science & Business Media,  
556 2012.
- 557 Zhengxue Cheng, Heming Sun, Masaru Takeuchi, and Jiro Katto. Energy compaction-based image  
558 compression using convolutional autoencoder. *IEEE Transactions on Multimedia*, 22(4):860–873,  
559 2019.
- 560 Fabio Duarte. Amount of data created daily (2024). [https://explodingtopics.com/  
561 blog/data-generated-per-day](https://explodingtopics.com/blog/data-generated-per-day), 2024. Accessed: 2024-07-14.
- 562  
563 Emilien Dupont, Adam Goliński, Milad Alizadeh, Yee Whye Teh, and Arnaud Doucet. Coin: Com-  
564 pression with implicit neural representations. *arXiv preprint arXiv:2103.03123*, 2021.
- 565 Emilien Dupont, Hrushikesh Loya, Milad Alizadeh, Adam Goliński, Yee Whye Teh, and Arnaud  
566 Doucet. Coin++: Neural compression across modalities. *arXiv preprint arXiv:2201.12904*, 2022.
- 567  
568 Robert M. Gray and David L. Neuhoff. Quantization. *IEEE transactions on information theory*, 44  
569 (6):2325–2383, 1998.
- 570 Zekun Hao, Arun Mallya, Serge Belongie, and Ming-Yu Liu. Implicit neural representations with  
571 levels-of-experts. *Advances in Neural Information Processing Systems*, 35:2564–2576, 2022.
- 572  
573 Daniel J Hsu, Sham M Kakade, John Langford, and Tong Zhang. Multi-label prediction via com-  
574 pressed sensing. *Advances in neural information processing systems*, 22, 2009.
- 575 Junlin Hu and Yap-Peng Tan. Nonlinear dictionary learning with application to image classification.  
576 *Pattern Recognition*, 75:282–291, 2018.
- 577  
578 Zhe Hu, Jia-Bin Huang, and Ming-Hsuan Yang. Single image deblurring with adaptive dictionary  
579 learning. In *2010 IEEE International Conference on Image Processing*, pp. 1169–1172. IEEE,  
580 2010.
- 581 Donghua Jiang, Nestor Tsafack, Wadii Boulila, Jawad Ahmad, and JJ Barba-Franco. Asb-cs: Adap-  
582 tive sparse basis compressive sensing model and its application to medical image encryption.  
583 *Expert Systems with Applications*, 236:121378, 2024.
- 584  
585 Gareth A Jones and J Mary Jones. *Information and coding theory*. Springer Science & Business  
586 Media, 2012.
- 587  
588 Ashish Kapoor, Raajay Viswanathan, and Prateek Jain. Multilabel classification using bayesian  
589 compressed sensing. *Advances in neural information processing systems*, 25, 2012.
- 590 Syed Ali Khayam. The discrete cosine transform (dct): theory and application. *Michigan State*  
591 *University*, 114(1):31, 2003.
- 592  
593 Li Liu and Paul Fieguth. Texture classification using compressed sensing. In *2010 Canadian Con-  
ference on Computer and Robot Vision*, pp. 71–78. IEEE, 2010.

- 594 Yang Liu, Qingchao Chen, Wei Chen, and Ian Wassell. Dictionary learning inspired deep network  
595 for scene recognition. In *Proceedings of the AAAI conference on artificial intelligence*, volume 32,  
596 2018.
- 597 Liyan Ma, Lionel Moisan, Jian Yu, and Tiejong Zeng. A dictionary learning approach for poisson  
598 image deblurring. *IEEE Transactions on medical imaging*, 32(7):1277–1289, 2013.
- 600 Ben Mildenhall, Pratul P Srinivasan, Matthew Tancik, Jonathan T Barron, Ravi Ramamoorthi, and  
601 Ren Ng. Nerf: Representing scenes as neural radiance fields for view synthesis. *Communications*  
602 *of the ACM*, 65(1):99–106, 2021.
- 603 AKM Rabby and Chengcui Zhang. Beyondpixels: A comprehensive review of the evolution of  
604 neural radiance fields. *arXiv preprint arXiv:2306.03000*, 2023.
- 606 AM Raid, WM Khedr, Mohamed A El-Dosuky, and Wesam Ahmed. Jpeg image compression using  
607 discrete cosine transform-a survey. *arXiv preprint arXiv:1405.6147*, 2014.
- 608 Sameera Ramasinghe and Simon Lucey. Beyond periodicity: Towards a unifying framework for acti-  
609 vations in coordinate-mlps. In *European Conference on Computer Vision*, pp. 142–158. Springer,  
610 2022.
- 612 Vishwanath Saragadam, Daniel LeJeune, Jasper Tan, Guha Balakrishnan, Ashok Veeraraghavan,  
613 and Richard G Baraniuk. Wire: Wavelet implicit neural representations. In *Proceedings of the*  
614 *IEEE/CVF Conference on Computer Vision and Pattern Recognition*, pp. 18507–18516, 2023.
- 616 K Seemakurthy, A Majumdar, J Gubbi, NK Sandeep, A Varghese, S Deshpande, M Girish Chandra,  
617 and P Balamurali. Deep dictionary learning for inpainting. In *Computer Vision, Pattern Recog-*  
618 *niton, Image Processing, and Graphics: 7th National Conference, NCVPRIPG 2019, Hubballi,*  
619 *India, December 22–24, 2019, Revised Selected Papers 7*, pp. 79–88. Springer, 2020.
- 620 Aviv Shamsian, Aviv Navon, David W Zhang, Yan Zhang, Ethan Fetaya, Gal Chechik, and Haggai  
621 Maron. Improved generalization of weight space networks via augmentations. *arXiv preprint*  
622 *arXiv:2402.04081*, 2024.
- 624 Vincent Sitzmann, Julien Martel, Alexander Bergman, David Lindell, and Gordon Wetzstein. Im-  
625 plicit neural representations with periodic activation functions. *Advances in neural information*  
626 *processing systems*, 33:7462–7473, 2020.
- 627 Stanford University Computer Graphics Laboratory. The stanford 3d scanning repository. <https://graphics.stanford.edu/data/3Dscanrep/>. Accessed: 2024-07-15.
- 628 Yannick Strümpfer, Janis Postels, Ren Yang, Luc Van Gool, and Federico Tombari. Implicit neural  
629 representations for image compression. In *European Conference on Computer Vision*, pp. 74–91.  
630 Springer, 2022.
- 633 Matthew Tancik, Pratul Srinivasan, Ben Mildenhall, Sara Fridovich-Keil, Nithin Raghavan, Utkarsh  
634 Singhal, Ravi Ramamoorthi, Jonathan Barron, and Ren Ng. Fourier features let networks learn  
635 high frequency functions in low dimensional domains. *Advances in neural information processing*  
636 *systems*, 33:7537–7547, 2020.
- 637 Hao Tang, Hong Liu, Wei Xiao, and Nicu Sebe. When dictionary learning meets deep learning:  
638 Deep dictionary learning and coding network for image recognition with limited data. *IEEE*  
639 *transactions on neural networks and learning systems*, 32(5):2129–2141, 2020.
- 641 Lucas Theis, Wenzhe Shi, Andrew Cunningham, and Ferenc Huszár. Lossy image compression with  
642 compressive autoencoders. In *International conference on learning representations*, 2022.
- 643 Joel A Tropp and Anna C Gilbert. Signal recovery from random measurements via orthogonal  
644 matching pursuit. *IEEE Transactions on information theory*, 53(12):4655–4666, 2007.
- 646 Gregory K Wallace. The jpeg still picture compression standard. *IEEE transactions on consumer*  
647 *electronics*, 38(1):xviii–xxxiv, 1992.

648 Xijuan Zhang, Oscar L Olvera Astivia, Edward Kroc, and Bruno D Zumbo. How to think clearly  
649 about the central limit theorem. *Psychological Methods*, 2022.  
650

651 Hongyi Zheng, Hongwei Yong, and Lei Zhang. Deep convolutional dictionary learning for image  
652 denoising. In *Proceedings of the IEEE/CVF conference on computer vision and pattern recogni-*  
653 *tion*, pp. 630–641, 2021.

654 Jinjia Zhou and Jian Yang. Compressive sensing in image/video compression: Sampling, coding,  
655 reconstruction, and codec optimization. *Information*, 15(2):75, 2024.  
656

657 Fang Zhu, Shuai Guo, Li Song, Ke Xu, Jiayu Hu, et al. Deep review and analysis of recent nerfs.  
658 *APSIPA Transactions on Signal and Information Processing*, 12(1), 2023.  
659  
660  
661  
662  
663  
664  
665  
666  
667  
668  
669  
670  
671  
672  
673  
674  
675  
676  
677  
678  
679  
680  
681  
682  
683  
684  
685  
686  
687  
688  
689  
690  
691  
692  
693  
694  
695  
696  
697  
698  
699  
700  
701